Physics Letters B 741 (2015) 246–251

Contents lists available at ScienceDirect

Physics Letters B

www.elsevier.com/locate/physletb

Geometrical scaling and the dependence of the average transverse momentum on the multiplicity and energy for the ALICE experiment

Larry McLerran [a,b,c], Michal Praszalowicz [d,*]

[a] Physics Dept., Bldg. 510A, Brookhaven National Laboratory, Upton, NY 11973, USA
[b] RIKEN BNL Research Center, Bldg. 510A, Brookhaven National Laboratory, Upton, NY 11973, USA
[c] Physics Department, China Central Normal University, Wuhan 430079, China
[d] M. Smoluchowski Institute of Physics, Jagiellonian University, S. Lojasiewicza 11, 30-348 Krakow, Poland

ARTICLE INFO

Article history:
Received 31 July 2014
Received in revised form 19 November 2014
Accepted 21 December 2014
Available online 24 December 2014
Editor: J.-P. Blaizot

ABSTRACT

We review the recent ALICE data on charged particle multiplicity in p–p collisions, and show that it exhibits Geometrical Scaling (GS) with energy dependence given with characteristic exponent $\lambda = 0.22$. Next, starting from the GS hypothesis and using results of the Color Glass Condensate effective theory, we calculate $\langle p_T \rangle$ as a function N_{ch} including dependence on the scattering energy W. We show that $\langle p_T \rangle$ both in p–p and p–Pb collisions scales in terms of scaling variable $(W/W_0)^{\lambda/(2+\lambda)}\sqrt{N_{ch}/S_\perp}$ where $S_\perp$ is multiplicity-dependent interaction area in the transverse plane. Furthermore, we discuss how the behavior of the interaction radius R at large multiplicities affects the mean p_T dependence on N_{ch}, and make a prediction that $\langle p_T \rangle$ at high multiplicity should reach an energy-independent limit.

Recently, the ALICE Collaboration has published charged particle spectra from p–p collisions at three LHC energies 0.9, 2.76 and 7 TeV. This data, together with p–Pb and Pb–Pb data has been subsequently used to construct other quantities, in particular total multiplicity and mean p_T as a function of charged particle multiplicity N_{ch} [1,2]. This dependence has been next tested against hypothesis of Geometrical Scaling (GS) proposed in Ref. [3] with a conclusion that "ALICE p–p and p–Pb data at low and intermediate multiplicities are compatible with the proposed scaling" with substantial departure from scaling at larger multiplicities [2]. In this Letter we show that GS works in fact much better, provided one takes into account energy dependence of the interaction radius at fixed multiplicity.

The paper is organized as follows. First we introduce the basic concepts of Geometrical Scaling for p_T spectra and show that the ALICE data exhibit GS over a limited rage of p_T with energy dependence determined by the characteristic exponent $\lambda = 0.22$. This value is slightly lower than the one found from the analysis [4] of single non-diffractive CMS data [5], and the one found [6] in Deep Inelastic Scattering (DIS) [7]. Next, we derive the formula for mean transverse momentum and discuss multiplicity dependence of the interaction radius. We use results of the calculations [8] performed within the Color Glass Condensate (CGC) effective theory [9]. Finally we discuss the energy dependence of the interaction radius and show that very good scaling of mean p_T is seen in the ALICE data. We also argue that the character of the energy dependence changes for large multiplicities where the interaction radius should reach energy-independent value. Such behavior has testable phenomenological consequences. We finish with conclusions.

Multi-particle production at low and moderate transverse momenta probes the nonperturbative regime of Quantum Chromodynamics (QCD). Yet at high energies an overall picture drastically simplifies due to the existence of an intermediate energy scale, the saturation momentum $Q_s(x)$. Particle production proceeds via gluon scattering whose distribution is determined by the ratio $p_T/Q_s(x)$ where Bjorken x corresponds to the longitudinal gluon momentum. Therefore, on dimensional grounds, the gluon multiplicity distribution is given in terms of the universal function $\mathcal{F}(\tau)$ [11–13]

$$\frac{dN_g}{dyd^2p_T} = S_\perp \mathcal{F}(\tau) \tag{1}$$

where

$$\tau = \frac{p_T^2}{Q_s^2(x)} \tag{2}$$

* Corresponding author.
E-mail addresses: mclerran@me.com (L. McLerran), michal@if.uj.edu.pl (M. Praszalowicz).

http://dx.doi.org/10.1016/j.physletb.2014.12.046

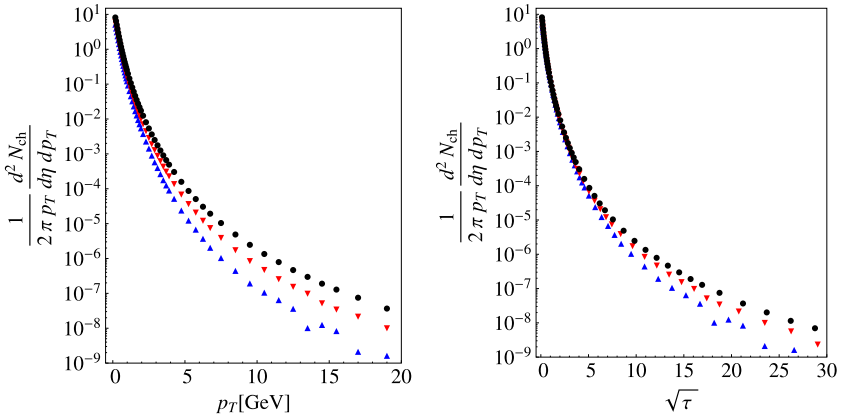

Fig. 1. Multiplicity distribution of charged particles in p–p collisions at 0.9 TeV (blue up-triangles), 2.76 TeV (red down-triangles) and 7 TeV (black full circles) plotted as functions of $p_{\rm T}$ (left) and as functions of the scaling variable $\sqrt{\tau}$ for $\lambda = 0.22$ (right). (For interpretation of the references to color in this figure legend, the reader is referred to the web version of this article.)

is the scaling variable. Here

$$Q_s^2(x) = Q_0^2\left(\frac{x_0}{x}\right)^{\lambda} \tag{3}$$

is the saturation momentum, Q_0 is an arbitrary scale parameter for which we take 1 GeV/c, and for x_0 we take 10^{-3}. Our analysis of GS presented in the present paper is not sensitive to the actual value of x_0 and/or Q_0, but only to the value of λ. Bjorken x's of colliding partons for mid rapidity production take the following form

$$x = \frac{p_{\rm T}}{W}. \tag{4}$$

Here $W = \sqrt{s}$ is the scattering energy and $S_\perp$ is a transverse area which will be specified later. Eq. (1) exemplifies the property of the particle spectra known as Geometrical Scaling (GS) where an observable that in principle depends on two kinematical variables, such as $p_{\rm T}$ and W (or Bjorken x), depends in practice on a specific combination of them through the scaling variable. In Eq. (1) we have suppressed strong coupling constant α_s whose dependence on $p_{\rm T}$ is expected to introduce weak GS violation.

Eq. (1) applies to the scattering of symmetric systems (pp, AA). For pA scattering, which we will also discuss here, there are in principle two saturation scales: the one of the proton $Q_s^{(\rm p)} = Q_{\rm p}$, and that of the nucleus, $Q_s^{(A)} = Q_A$ [14,15]. This issue has been discussed in Ref. [3] with a conclusion that for high enough multiplicities and for central rapidities the two scales should have the same energy dependence, meaning that $Q_{\rm p}/Q_A = \text{const}$. This condition is enough for GS of the form (1) to hold for pA collisions as well. A test of this assumption will be provided by the forthcoming pA data at a different LHC energy.

Geometrical scaling [16] has been introduced in the context of DIS at HERA and later extended to particle production in hadronic collisions [4,17,18]. The saturation scale appears due to the nonlinear effects in parton evolution with growing energy. This evolution is in general described by the JIMWLK equation [19] which for large $N_{\rm c}$ reduces to the Balitsky–Kovchegov equation [20]. These equations possess traveling wave solutions which explicitly exhibit GS [21].

A good description of large energy scattering, or equivalently of small Bjorken x's, is the effective field theory [9] of the Color Glass Condensate (CGC) (for an introduction and review see Ref. [10]). In the theory of the CGC, hadrons after a collision stretch in the longitudinal direction strong gluonic fields that are coherent in the transverse plane over the radius $1/Q_{\rm s}$. Multi-particle production proceeds by the decay of these flux tubes, and it has been shown that the dominant contribution comes from the production of gluons with $p_{\rm T} \le Q_{\rm s}$. This mechanism is able to explain different features of high energy p–p collisions including *e.g.* negative binomial distribution [22] or ridge correlations in high multiplicity events [23]. In this paper we shall use predictions of the CGC effective theory for the interaction radii as functions of gluon multiplicity in p–p and p–Pb collisions discussed in Ref. [8].

An immediate consequence of Eq. (1) is that $p_{\rm T}$ spectra at different energies fall on one universal curve if plotted in terms of the scaling variable τ.[1] The quality of GS depends on the value of the exponent λ entering the definition of the saturation scale (3). In order to determine λ in a model-independent way we employ a method of ratios where we construct

$$\mathcal{R}_{ik}(\tau) = \frac{dN(W_i,\tau)}{dyd^2p_{\rm T}} \Big/ \frac{dN(W_k,\tau)}{dyd^2p_{\rm T}} \tag{5}$$

which, according to (1), should be equal to unity if GS is present. In practice $R_{ik} \approx 1$ in a window $\tau_{\rm min} < \tau < \tau_{\rm max}$. For particles of small $p_{\rm T}$ (*i.e.* small τ), comparable to $\Lambda_{\rm QCD}$ and/or pion mass, we do not expect the arguments that lead to GS to be applicable, and for large $p_{\rm T}$ we enter into a domain of large Bjorken x's (4) where GS is explicitly violated and perturbative QCD takes over. In Eq. (5) we have assumed that the number of charged particles is proportional to the number of produced gluons and the proportionally factor does not depend on energy (so-called parton–hadron duality). We have checked by explicit calculations of mean square deviations of $\mathcal{R}_{ik}$'s from unity that the best value of λ for the ALICE data that gives the smallest χ^2 over the largest interval in τ is equal to 0.22 [24]. This is illustrated in Fig. 1 where in the left panel we plot $dN/dyd^2p_{\rm T}$ as functions of $p_{\rm T}$ and as functions of $\sqrt{\tau}$ for $\lambda = 0.22$ (right panel). We see that spectra at different energies overlap within a window up to $\sqrt{\tau} \sim 4$. In order not to be biased by the logarithmic scale of Fig. 1, we construct two ratios $\mathcal{R}_{12}$ and $\mathcal{R}_{13}$ corresponding to the LHC energies $W_1 = 7$, $W_2 = 2.76$ and $W_3 = 0.9$ TeV, respectively. These ratios are plotted in Fig. 2 where again we plot them as functions of $p_{\rm T}$ (left panel) and as functions of $\sqrt{\tau}$ (right panel). We see relatively good scaling where the weak rise R_{ik}'s with $\sqrt{\tau}$ can be attributed to the residual dependence of λ upon $p_{\rm T}^2$ [17].

The behavior of ratios $\mathcal{R}_{ik}$ shown in Fig. 2 is almost identical as in the case of the CMS data analyzed in Ref. [4]. However we

[1] In what follows we shall use $\sqrt{\tau}$ which for $\lambda = 0$ reduces to $p_{\rm T}/Q_0$.

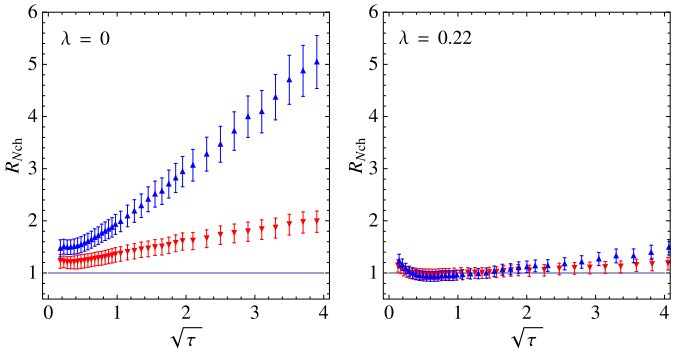

Fig. 2. Ratios $\mathcal{R}_{12}$ (*i.e.* 7 TeV to 2.76 TeV – red down-triangles) and $\mathcal{R}_{13}$ (*i.e.* 7 TeV to 0.9 TeV – blue up-triangles) plotted as functions of p_T (left) and as functions of scaling variable $\sqrt{\tau}$ for $\lambda = 0.22$ (right). (For interpretation of the references to color in this figure legend, the reader is referred to the web version of this article.)

have found in [4] that $\lambda_{CMS} = 0.27$ rather than 0.22 and that the GS window extends to slightly higher τ. This may be due to the different event selection (single non-diffractive at CMS vs. inelastic in ALICE) and different pseudo rapidity coverage ($|\eta| < 2.4$ at CMS vs. $|\eta| < 0.3$ at ALICE). In a recent study of GS in prompt photon production [25] the optimal range of λ turned out to be 0.22–0.28. These differences in λ maybe in fact due to some additional weak energy dependence of the multiplicity distribution (1), like the one of α_s or some energy dependence of the unintegrated glue. Moreover one should bare in mind that there is no factorization theorem for multiparticle production in k_T-dependent gluon density formalism. Studying ALICE data we have found for example [24], that better GS quality is achieved for the differential cross-section, rather than for the multiplicity, with $\lambda \sim 0.32$. Further discussion of these issues will be presented elsewhere [24].

Having established the existence of GS in the ALICE data we can now proceed to the analysis of total multiplicity and $\langle p_T \rangle$. In order to calculate integrals over p_T we need a Jacobian:

$$p_T = \bar{Q}_s(W)\,\tau^{1/(2+\lambda)},$$
$$dp_T^2 = \frac{2}{2+\lambda}\bar{Q}_s^2(W)\tau^{-\lambda/(2+\lambda)}d\tau, \tag{6}$$

where we have introduced an *average* saturation scale

$$\bar{Q}_s(W) = Q_0\left(\frac{W}{Q_0}\right)^{\lambda/(2+\lambda)}, \tag{7}$$

which can be thought of as a solution of the equation

$$Q_s^2(\bar{Q}_s/W) = \bar{Q}_s^2. \tag{8}$$

Note that due to our choice of $x_0 = 10^{-3}$ in Eq. (3) p_T and Q_0 in Eq. (7) are in GeV and W is in TeV.

It follows that

$$\frac{dN_g}{dy} = A\,S_\perp \bar{Q}_s^2(W) \tag{9}$$

where A is an integral over the universal function $\mathcal{F}(\tau)$

$$A = \frac{2\pi}{2+\lambda}\int \tau^{-\frac{\lambda}{2+\lambda}}\mathcal{F}(\tau)d\tau \tag{10}$$

and as such is energy-independent. The constant A can, however, depend on particle species produced in the collision.

The universal function $\mathcal{F}(\tau)$ is not known from first principles, however, in most phenomenological applications where good description of the p_T spectra is given in terms of Tsallis parametrization, one can show that [26]

$$\mathcal{F}(\tau) \sim \left(1 + \frac{\tau^{1/(2+\lambda)}}{n\kappa}\right)^{-n} \xrightarrow[\tau\to\infty]{} \left(\frac{n\kappa}{\tau^{1/(2+\lambda)}}\right)^n. \tag{11}$$

Here constant κ follows from the fits to the transverse momentum spectra and it is of the order of 0.1 [3], and power n is of the order 5–9. In what follows we shall need this explicit form of $\mathcal{F}(\tau)$ only to estimate possible energy dependence of its integrals, such as A of Eq. (9), coming from the fact that experimentally p_T spectra are measured up to some p_T^{max} which translates into the maximal τ_{max}

$$\tau_{max} = \left(\frac{p_T^{max}}{Q_0}\right)^{2+\lambda}\left(\frac{Q_0}{W}\right)^{\lambda}, \tag{12}$$

which is energy-dependent. Here again p_T and Q_0 in Eq. (12) are in GeV and W is in TeV. It follows that for the ALICE data $\tau_{max} \approx 700$, 1300 and 1700 for scattering energies $W = 0.9, 2.76$ and 7 TeV, respectively. Since n is here numerically the highest power, the contributions of the unphysical tail, *i.e.* from $\tau > \tau_{max}$, are dumped approximately as $(1/\tau_{max})^{n/2-1}$ multiplied by a small coefficient $(n\kappa)^n$. Therefore in what follows we shall neglect finite energy effects on the integrals of $\mathcal{F}(\tau)$. We have checked numerically that the contribution to the mean transverse momentum coming from this effect is at the per mille level.

Eq. (9) can be though of as a definition of the saturation scale, which is essentially given as gluon number density per transverse area. One should however keep in mind that the transverse area itself does depend on multiplicity as well, since it corresponds to the overlap area of two colliding systems at fixed impact parameter b. The smaller b the larger $S_\perp$. This dependence will be of importance in the following, where we discuss mean p_T dependence on multiplicity.

It follows from Eq. (9) that particle multiplicity in mid rapidity grows like a power of the scattering energy, which is in remarkable agreement with the LHC data [27]. The power of this growth is solely given by the energy rise of the average saturation scale $\bar{Q}_s^2$. Numerically for $\lambda = 0.22$, we find that $\lambda/(2+\lambda) \simeq 0.099$, which again is in agreement with experimental results [27]. From this simple analysis we conclude that $S_\perp$ is energy-independent over the LHC energy range (or very weakly dependent for larger energy span).

When this formula is applied to minimum bias hadron–hadron collisions, we are basically fixing the average hadron radius. This average radius seems to be a slowly varying function of energy. However, and this will be of primary importance in the following, if we *fix* dN_g/dy and then *change* energy, then $S_\perp$ has to change with energy as well in agreement with Eq. (9). This is because different radii are sampled at the different impact parameters. If we vary the density of particle per unit area, by varying the saturation momentum, and then require fixed multiplicity, we necessarily will sample different impact parameters corresponding to different areas.

In heavy ion collisions $S_\perp$ is equal to the geometrical transverse size of the overlap of the colliding nuclei. As such it is related to the centrality of the event and, in consequence, to the event multiplicity. It is less clear what is geometrical interpretation of $S_\perp$ in p–p collisions. In a model with an impact parameter dependent saturation scale $Q_s^b(b_\perp)$ [29] we have:

$$\bar{Q}_s^2 S_\perp = \int d^2r_\perp Q_s^b(r_\perp)^2, \tag{13}$$

where the integral extends over the overlap area $S_\perp$ of colliding protons at a given impact parameter b. It is therefore obvious that also in the case of p–p scattering there should be a relation between $S_\perp$ and multiplicity in a given event. Indeed, this dependence has been calculated within the CGC framework [8], which

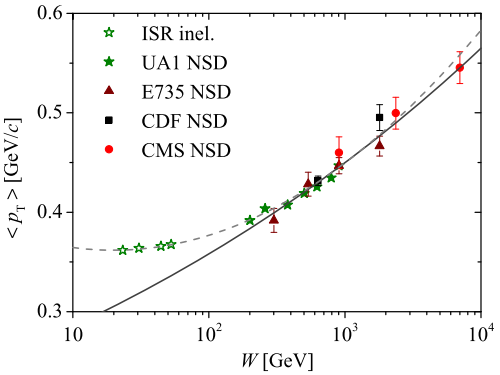

Fig. 3. Energy dependence of mean p_T. Compilation of data from Ref. [28]. Solid line corresponds to the power law behavior of Eq. (14): $0.227 \times W^{0.099}$, while the dashed line corresponds to the CMS logarithmic fit aimed at describing also low energy data: $0.413 - 0.0171 \ln s + 0.00143 \ln^2 s$, with $W^2 = s$.

predicts that $S_\perp$ depends on $N_{\rm ch}^{2/3}$ linearly, and then saturates at some constant value. This behavior has a simple geometrical interpretation: number of particles produced in hadronic collisions is proportional to the active overlap volume. Once the maximal volume is reached, further growth of multiplicity is due solely to fluctuations.

Average p_T can be easily calculated using Eqs. (1) and (6) giving

$$\langle p_T \rangle = \frac{\int p_T \frac{dN_g}{dyd^2p_T} d^2p_T}{\int \frac{dN_g}{dyd^2p_T} d^2p_T} = \bar{Q}_s(W) \frac{B}{A} \tag{14}$$

where

$$B = \frac{2\pi}{2+\lambda} \int d\tau \tau^{\frac{1-\lambda}{2+\lambda}} \mathcal{F}(\tau). \tag{15}$$

Eq. (14) has two important consequences. First, it gives right away the energy dependence of $\langle p_T \rangle$ which is illustrated in Fig. 3 where good agreement with the data taken from Ref. [28] can bee seen. Second, at some fixed energy W_0 one can express $\bar{Q}_s(W_0)$ in terms of the gluon multiplicity (9), which gives

$$\langle p_T \rangle|_{W_0} = \frac{B}{A} \sqrt{\frac{dN_g/dy}{AS_\perp (dN_g/dy)|_{W_0}}}. \tag{16}$$

Note that for fixed dN_g/dy interaction size $S_\perp$ in Eq. (16) depends, as explained above, on the reference energy W_0 and also on dN_g/dy itself, which is related to the number of charged particles $N_{\rm ch}$ in the kinematical range of a given experiment:

$$N_{\rm ch} = \frac{1}{\gamma \Delta y} \int_{\Delta y} \frac{dN_g}{dy} dy. \tag{17}$$

Here the coefficient γ relates gluon multiplicity to the multiplicity of observed charged hadrons within the rapidity interval Δy. For ALICE data used in this paper $\Delta y = 0.6$. The interaction radius R characterizing the volume from which the particles are produced and which is related to $S_\perp = \pi R^2$, depends in a natural way on the third root of dN_g/dy, *i.e.* $R = R(\sqrt[3]{dN_g/dy}) = R(\sqrt[3]{\gamma N_{\rm ch}})$ [8] and on the collision energy W_0.

In the following we shall use a slightly modified formula for $\langle p_T \rangle$, which takes into account nonperturbative effects and contributions from the particle masses encoded in a constant α:

$$\langle p_T \rangle|_{W_0} = \alpha + \beta \frac{\sqrt{N_{\rm ch}}}{R(\sqrt[3]{\gamma N_{\rm ch}})|_{W_0}}. \tag{18}$$

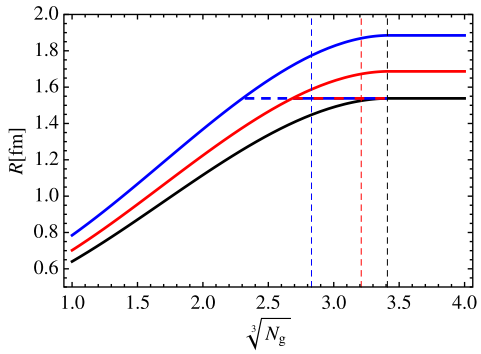

Fig. 4. $R(N_g^{1/3})$ for three different energies. The lowest solid (black) curve corresponds to the parametrization (19) at $W_0 = 7$ TeV, whereas two upper solid curves correspond to (19) multiplied by the energy-dependent factor $(W_0/W)^{\lambda/(2+\lambda)}$ for $W = 2.76$ TeV (red) and 0.9 TeV (blue). High multiplicity saturation is schematically depicted by dashed lines. Vertical thin dashed lines correspond to the highest multiplicities analyzed by the ALICE Collaboration at 0.9 TeV (most left blue), 2.76 TeV (middle red) and 7 TeV (most right black). (For interpretation of the references to color in this figure legend, the reader is referred to the web version of this article.)

Here α and β are constants that do not depend on energy. Formula (18) has been proven to work very well in p–p at 7 TeV and also in p–Pb collisions at 5.02 TeV at the LHC [3].

The interaction radius $R(\sqrt[3]{dN_g/dy})$ has been calculated in Ref. [8]. Here we shall use the parametrization of Ref. [3]:

$$R_{\rm pp}(x) = \begin{cases} 0.387 + 0.0335x \\ \quad + 0.274x^2 - 0.0542x^3 & \text{if } x < 3.4 \text{ [fm]}, \\ 1.538 & \text{if } x \geq 3.4 \end{cases} \tag{19}$$

for p–p collisions at 7 TeV and

$$R_{\rm pPb}(x) = \begin{cases} 0.21 + 0.47x & \text{if } x < 3.5 \\ 1.184 - 0.483x \\ \quad + 0.305x^2 - 0.032x^3 & \text{if } 3.5 \leq x < 5 \\ 2.394 & \text{if } x \geq 5 \end{cases} \text{ [fm]}, \tag{20}$$

for p–Pb collisions at 5.02 TeV.

In our analysis of the 7 TeV ALICE data, it turns out we are only sensitive to radii where we are in the first interval for the dependence of R on multiplicity. This is the region where impact parameter is varying. In the very high multiplicity region, the radius saturates and at lower energies it happens for lower multiplicities.

The energy dependence of (18) follows from the general form given by Eq. (14). In order to find an explicit formula for mean p_T at any scattering energy W, *i.e.* for $\langle p_T \rangle|_W$, one has to recompute $R(\sqrt[3]{\gamma N_{\rm ch}})$, but – as a consequence of Eq. (14) – one should obtain that

$$\begin{aligned} \langle p_T \rangle|_W &= \alpha + \beta \frac{\sqrt{N_{\rm ch}}}{R(\sqrt[3]{\gamma N_{\rm ch}})|_W} \\ &= \alpha + \beta \left(\frac{W}{W_0} \right)^{\lambda/(2+\lambda)} \frac{\sqrt{N_{\rm ch}}}{R(\sqrt[3]{\gamma N_{\rm ch}})|_{W_0}} \end{aligned} \tag{21}$$

where W_0 corresponds to the energy for which the interaction radius has been computed. For p–p $W_0 = 7$ TeV if we use $R_{\rm pp}$ from Eq. (19), and for p–Pb $W_0 = 5.02$ TeV corresponding to $R_{\rm pPb}$ of Eq. (20).

Eq. (21) implies that the effective interaction radius at fixed multiplicity varies with energy as $(W_0/W)^{\lambda/(2+\lambda)} R|_{W_0}$. This is depicted in Fig. 4 where we plot $R(N_g^{1/3})$ for three different energies.

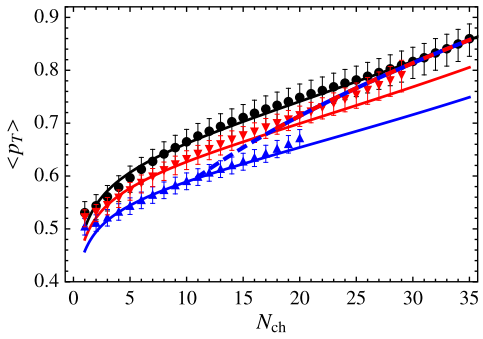

Fig. 5. Mean $\langle p_T \rangle$ in p–p collisions for three different LHC energies 7 TeV (full black circles), 2.76 TeV (full red down-triangles) and 0.9 TeV (full blue down-triangles) together with theoretical parametrizations of Eq. (21). Solid lines correspond to the interaction radii R shown in Fig. 4 as the solid lines as well, whereas dashed lines show the change in the multiplicity dependence caused by sharp R saturation shown in Fig. 4 as dashed lines. (For interpretation of the references to color in this figure legend, the reader is referred to the web version of this article.)

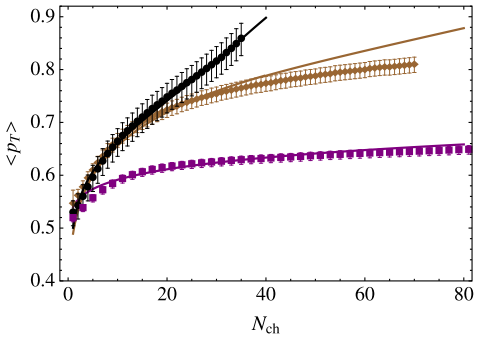

Fig. 6. Mean $\langle p_T \rangle$ in p–p collisions at 7 TeV (full black circles), in p–Pb collisions at 5.02 TeV (full brown diamonds) and in Pb–Pb collisions at 2.76 TeV (full purple squares) together with parametrizations of Eqs. (18) and (24). (For interpretation of the references to color in this figure legend, the reader is referred to the web version of this article.)

The lowest solid (black) curve corresponds to the parametrization (19) at $W_0 = 7$ TeV, whereas two upper solid curves correspond to (19) multiplied by the energy-dependent factor $(W_0/W)^{\lambda/(2+\lambda)}$ for $W = 2.76$ TeV (red) and 0.9 TeV (blue).

It is however clear that the power law increase of effective interaction radius at low energies has to tamed at some point. It is not possible in a model-independent way to find how this actually happens. Therefore we have assumed a simplistic model that radii at all energies saturate at about 1.5 fm, a value corresponding to the CGC prediction at 7 TeV. This is shown in Fig. 4 by dashed lines corresponding to the sharp cut-off of the interaction radii. Of course, the sharp cut-off is a very naive assumption and in reality the approach to radius saturation is certainly more complicated as suggested by the disagreement of the 0.9 TeV with fixed radius saturation hypothesis. This issue can be also addressed by reverting the logic and by extracting the interaction radius from the data. An attempt in this direction is briefly discussed in Ref. [30].

We can now check these ideas against experiment using ALICE data on p–p, p–Pb and Pb–Pb scattering [1,2]. Let us first consider the case where interaction radii at different energies saturate at different values corresponding to the solid lines in Fig. 4.

We have used the p–p data at 7 TeV as the reference fitting to it formula (18) with the following result:

$$\alpha = 0.268\ \text{GeV}, \qquad \beta = 0.153\ \text{GeV fm}, \qquad \gamma = 1.138. \tag{22}$$

One would naively expect

$$\gamma \simeq \frac{3}{2}\frac{1}{\Delta y}$$

which for ALICE pseudo-rapidity interval $|\eta| < 0.3$ would give 2.5 rather than 1.138. Predictions for other two LHC energies follow from Eq. (21) with no other parameters. The result is plotted in Fig. 5 and one can see good but not perfect agreement with the data. One can observe that the 2.76 TeV points (red down-triangles) at higher multiplicities tend towards the 7 TeV curve, and that two last 0.9 TeV points (blue up-triangles) seem to show the similar tendency. This behavior can be attributed to the fixed value saturation of R as depicted in Fig. 4 by the dashed lines. The effect of fixed R is shown by the dashed lines in Fig. 5. One can see that 2.76 TeV data follow quite closely the fixed saturation radius prediction starting from $N_{\rm ch} \sim 17$, whereas the 0.9 TeV are well below the dashed line.

It is important to note at this point that the fit leading to Eq. (22) is performed over the multiplicities measured at 7 TeV that correspond to the most right (black dashed) vertical line in Fig. 4. One can see that the fit is driven totally by the almost linear rise of R with $N_{\rm g}^{1/3}$ with some sensitivity to the curvature before saturation, and does not depend on the value of the saturation radius. On the contrary, lower energy data in fixed saturation radius scenario, are more sensitive both to the curvature and the value of the saturation radius for which, however, we do not have model calculation. Therefore our analysis can be only qualitative at this point. With more data at higher multiplicities one could make a global fit to disentangle the functional dependence of R on multiplicity in a model-independent way.

Analogously we can calculate $\langle p_T \rangle$ for p–Pb collisions using the same values of parameters (22) with $R = R_{\rm pPb}$ of Eq. (20). The result is plotted in Fig. 6. For comparison we also plot in Fig. 6 $\langle p_T \rangle$ for p–p collisions at 7 TeV.

Finally we would like to check if mean p_T in Pb–Pb can be also described by formula (18). Unfortunately there is no calculation of the interaction radius dependence on $dN_{\rm g}/dy$ for heavy ion collisions. Making the plausible assumption that

$$R_{\rm PbPb} = \text{const} \cdot \sqrt[3]{N_{\rm ch}} \tag{23}$$

which simply states that the saturation radius where formula (23) should flatten is much larger than in the case of p–p and p–Pb collisions, and should not play any role in the region where data for the latter reactions are available. We have performed a fit to the Pb–Pb data using the following formula

$$\langle p_T \rangle_{\rm PbPb} = \alpha_{\rm PbPb} + \beta_{\rm PbPb}\frac{\sqrt{N_{\rm ch}}}{\sqrt[3]{N_{\rm ch}}} \tag{24}$$

obtaining

$$\alpha_{\rm PbPb} = 0.43\ \text{GeV}, \qquad \beta_{\rm PbPb} = 0.11\ \text{GeV}. \tag{25}$$

The data and the fit are also plotted in Fig. 6.

Yet another illustration of the mean p_T scaling is shown in Fig. 7 where we plot $\langle p_T \rangle$ as a function of the scaling variable $(W/W_0)^{\lambda/(2+\lambda)}\sqrt{N_{\rm ch}/S_\perp}$ both for p–p and p–Pb collisions. We see quite satisfactory scaling in contrary to the claim of Ref. [2] where the scaling variable has not been rescaled by the energy factor $(W/W_0)^{\lambda/(2+\lambda)}$. We cannot superimpose the Pb–Pb data on the plot in Fig. 7 because we do not know the absolute normalization of $R_{\rm PbPb}$ (23), which can be found only by explicit calculation within the CGC effective theory.

From this simple exercise we may conclude that mean p_T dependence on charged particle multiplicity can be well described in an approach based on the Color Glass Condensate and Geometrical Scaling. More understanding is certainly required as far as heavy

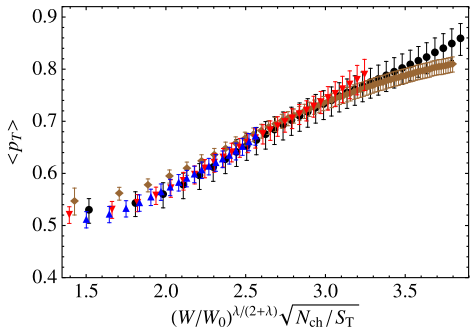

Fig. 7. Mean $\langle p_T \rangle$ in p–p collisions at 7 TeV (full black circles), 2.76 TeV (full red down-triangles), 0.9 TeV (full blue up-triangles) and in p–Pb collisions at 5.02 TeV (full brown diamonds) plotted in terms of scaling variable $(W/W_0)^{\lambda/(2+\lambda)}\sqrt{N_{ch}/S_\perp}$. For p–p $W_0 = 7$ TeV and for p–Pb $W_0 = 5.02$ TeV. (For interpretation of the references to color in this figure legend, the reader is referred to the web version of this article.)

ion data are concerned, although an onset of GS in nuclear collisions has been already reported [18,25]. We have established that ALICE data on charged particle multiplicity in p–p collisions exhibit Geometrical Scaling within a reasonable window in scaling variable τ with exponent $\lambda = 0.22$. There are some differences in the value of λ extracted from different experiments and different reactions, however, all results fall within a window 0.22–0.32. Further studies to understand these fine effects are clearly needed. The main finding of the present work concerns the energy dependence of $\langle p_T \rangle$ which is given by the energy dependence of the average saturation scale $\bar{Q}_s(W)$. Our final plot, Fig. 7, demonstrates very good scaling of $\langle p_T \rangle$ both in p–p and p–Pb collisions. New results at higher energies, especially in the case of p–Pb, will provide an important test of these ideas.

We have also argued that the interaction radii at different energies should for large multiplicities converge to some fixed value. Such tendency is clearly seen at 2.76 TeV and presumably at 0.9 TeV at multiplicities above 20. Our simplistic sharp cut-off model fails to describe 0.9 TeV data, but that could be presumably cured not affecting the other energies, by allowing for a somewhat larger value of the saturation radius and careful modeling of the curvature before saturation. We find it quite unexpected that such simple observable as $\langle p_T \rangle$ can provide such nontrivial information on the energy and multiplicity behavior of the interaction radius.

Acknowledgements

This research of M.P. has been supported by the Polish NCN grant 2011/01/B/ST2/00492. The research of L.M. is supported under DOE Contract No. DE-AC02-98CH10886.

References

[1] B.B. Abelev, et al., ALICE Collaboration, Eur. Phys. J. C 73 (2013) 2662, arXiv:1307.1093 [nucl-ex].
[2] B.B. Abelev, et al., ALICE Collaboration, Phys. Lett. B 727 (2013) 371, arXiv:1307.1094 [nucl-ex].
[3] L. McLerran, M. Praszalowicz, B. Schenke, Nucl. Phys. A 916 (2013) 210, arXiv:1306.2350 [hep-ph].
[4] L. McLerran, M. Praszalowicz, Acta Phys. Pol. B 41 (2010) 1917, arXiv:1006.4293 [hep-ph];
L. McLerran, M. Praszalowicz, Acta Phys. Pol. B 42 (2011) 99, arXiv:1011.3403 [hep-ph].
[5] V. Khachatryan, et al., CMS Collaboration, J. High Energy Phys. 1002 (2010) 041, arXiv:1002.0621 [hep-ex];
V. Khachatryan, et al., CMS Collaboration, Phys. Rev. Lett. 105 (2010) 022002, arXiv:1005.3299 [hep-ex].
[6] M. Praszalowicz, T. Stebel, J. High Energy Phys. 1303 (2013) 090, arXiv:1211.5305 [hep-ph].
[7] C. Adloff, et al., H1 Collaboration, Eur. Phys. J. C 21 (2001) 33, arXiv:hep-ex/0012053;
S. Chekanov, et al., ZEUS Collaboration, Eur. Phys. J. C 21 (2001) 443, arXiv:hep-ex/0105090.
[8] A. Bzdak, B. Schenke, P. Tribedy, R. Venugopalan, Phys. Rev. C 87 (2013) 064906, arXiv:1304.3403 [nucl-th].
[9] L.D. McLerran, R. Venugopalan, Phys. Rev. D 49 (1994) 2233, arXiv:hep-ph/9309289;
L.D. McLerran, R. Venugopalan, Phys. Rev. D 49 (1994) 3352, arXiv:hep-ph/9311205;
L.D. McLerran, R. Venugopalan, Phys. Rev. D 50 (1994) 2225, arXiv:hep-ph/9402335.
[10] K. Fukushima, Acta Phys. Pol. B 42 (2011) 2697, arXiv:1111.1025 [hep-ph].
[11] D. Kharzeev, M. Nardi, Phys. Lett. B 507 (2001) 121, arXiv:nucl-th/0012025.
[12] D. Kharzeev, E. Levin, Phys. Lett. B 523 (2001) 79, arXiv:nucl-th/0108006.
[13] D. Kharzeev, E. Levin, M. Nardi, Nucl. Phys. A 730 (2004) 448, arXiv:hep-ph/0212316;
D. Kharzeev, E. Levin, M. Nardi, Nucl. Phys. A 743 (2004) 329 (Erratum);
D. Kharzeev, E. Levin, M. Nardi, Nucl. Phys. A 747 (2005) 609, arXiv:hep-ph/0408050;
D. Kharzeev, E. Levin, M. Nardi, Phys. Rev. C 71 (2005) 054903, arXiv:hep-ph/0111315.
[14] Y.V. Kovchegov, A.H. Mueller, Nucl. Phys. B 529 (1998) 451, arXiv:hep-ph/9802440.
[15] A. Dumitru, L.D. McLerran, Nucl. Phys. A 700 (2002) 492, arXiv:hep-ph/0105268.
[16] A.M. Stasto, K.J. Golec-Biernat, J. Kwiecinski, Phys. Rev. Lett. 86 (2001) 596, arXiv:hep-ph/0007192.
[17] M. Praszalowicz, Phys. Rev. Lett. 106 (2011) 142002, arXiv:1101.0585 [hep-ph].
[18] M. Praszalowicz, Acta Phys. Pol. B 42 (2011) 1557, arXiv:1104.1777 [hep-ph];
M. Praszalowicz, in: Proceedings of the 47th Rencontres de Moriond, La Thuile, 2012, p. 265, arXiv:1205.4538 [hep-ph].
[19] J. Jalilian-Marian, A. Kovner, A. Leonidov, H. Weigert, Nucl. Phys. B 504 (1997) 415, arXiv:hep-ph/9701284;
J. Jalilian-Marian, A. Kovner, A. Leonidov, H. Weigert, Phys. Rev. D 59 (1998) 014014, arXiv:hep-ph/9706377;
E. Iancu, A. Leonidov, L.D. McLerran, Nucl. Phys. A 692 (2001) 583, arXiv:hep-ph/0011241;
E. Ferreiro, E. Iancu, A. Leonidov, L.D. McLerran, Nucl. Phys. A 703 (2002) 489, arXiv:hep-ph/0109115.
[20] I. Balitsky, Nucl. Phys. B 463 (1996) 99, arXiv:hep-ph/9509348;
Y.V. Kovchegov, Phys. Rev. D 60 (1999) 034008, arXiv:hep-ph/9901281;
Y.V. Kovchegov, Phys. Rev. D 61 (2000) 074018, arXiv:hep-ph/9905214.
[21] S. Munier, R.B. Peschanski, Phys. Rev. Lett. 91 (2003) 232001, arXiv:hep-ph/0309177;
S. Munier, R.B. Peschanski, Phys. Rev. D 69 (2004) 034008, arXiv:hep-ph/0310357.
[22] F. Gelis, T. Lappi, L. McLerran, Nucl. Phys. A 828 (2009) 149, arXiv:0905.3234 [hep-ph].
[23] A. Dumitru, K. Dusling, F. Gelis, J. Jalilian-Marian, T. Lappi, R. Venugopalan, Phys. Lett. B 697 (2011) 21, arXiv:1009.5295 [hep-ph].
[24] A. Francuz, M. Praszalowicz, in preparation.
[25] C. Klein-Bösing, L. McLerran, Phys. Lett. B 734 (2014) 282, arXiv:1403.1174 [nucl-th].
[26] M. Praszalowicz, Phys. Lett. B 727 (2013) 461, arXiv:1308.5911 [hep-ph].
[27] K. Aamodt, et al., ALICE Collaboration, Eur. Phys. J. C 65 (2010) 111, arXiv:0911.5430 [hep-ex].
[28] V. Khachatryan, et al., CMS Collaboration, Phys. Rev. Lett. 105 (2010) 022002, arXiv:1005.3299 [hep-ex].
[29] P. Tribedy, R. Venugopalan, Nucl. Phys. A 850 (2011) 136, arXiv:1011.1895 [hep-ph];
P. Tribedy, R. Venugopalan, Nucl. Phys. A 859 (2011) 185 (Erratum).
[30] M. Praszalowicz, arXiv:1410.5220 [hep-ph].